Mechanisms of Inhibition of Amido Phosphoribosyltransferase from Mouse L1210 Leukemia Cells†

Sarah L. Schoettle, Leesa B. Crisp, Eve Szabados, and Richard I. Christopherson*

Department of Biochemistry, University of Sydney, Sydney, New South Wales 2006, Australia

Received October 16, 1996; Revised Manuscript Received February 6, 1997[⊗]

ABSTRACT: Amido phosphoribosyltransferase (amido PRTase) catalyses the first step of the pathway for *de novo* biosynthesis of purine nucleotides. The enzyme is subject to inhibition by purine nucleoside 5′-monophosphates (AMP, IMP, and GMP), by dihydrofolate polyglutamates, and by the antifolate piritrexim [Sant, M. E., Lyons, S. D., Phillips, L., & Christopherson, R. I. (1992) *J. Biol. Chem. 267*, 11038−11045). Using a coupled radioassay, we have determined the substrate dissociation constants as 80.4 ± 13.2 μM for 5-phosphoribosyl 1-pyrophosphate (P-Rib-PP) and 421 ± 193 μM for L-glutamine with P-Rib-PP bound first with positive cooperativity for interaction with a second site on the catalytically active dimer (interaction factor of 0.247 ± 0.042). Analysis of inhibition patterns for amido PRTase shows that the antifolate piritrexim is a noncompetitive inhibitor bound with positive cooperativity at two allosteric sites of an inactive dimer with a dissociation constant of 66.0 ± 17.8 μM for interaction with the free enzyme and an interaction factor of 0.187 ± 0.113 with P-Rib-PP as the varied substrate. With L-glutamine as the varied substrate, a dissociation constant of 62.3 ± 15.6 μM for interaction with the enzyme−P-Rib-PP complex and an interaction factor of 0.0958 ± 0.0585 μM were obtained. AMP binds as a competitive inhibitor with respect to P-Rib-PP with a dissociation constant of 40.0 ± 8.1 μM for interaction with the free enzyme and as a noncompetitive inhibitor with respect to L-glutamine with a dissociation constant of 16.4 ± 5.2 mM for interaction with the enzyme−P-Rib-PP complex. Sucrose density gradient centrifugation of partially purified amido PRTase showed three molecular forms of the enzyme: an inactive tetramer (10.2 S) formed in the presence of AMP, an active dimer (6.7 S) formed with P-Rib-PP, and an inactive dimer (7.2 S) with piritrexim. The latter species may predominate in cells containing high levels of dihydrofolate polyglutamates.

Amido PRTase[1] catalyzes the first reaction of the *de novo* pathway for biosynthesis of purine nucleotides.

$$\text{P-Rib-PP} + \text{L-glutamine} \rightarrow \text{PRA} + \text{L-glutamate} + \text{PP}_i \quad (1)$$

Amido PRTase was initially purified to apparent homogeneity from chicken liver (Hartman, 1963), and a molecular mass of 210 kDa was determined from sedimentation and diffusion measurements. More recently, the amino acid sequences derived from the cDNAs encoding chicken, rat, and human amido PRTases have been used to calculate subunit molecular masses of 56 309, 57 436, and 57 447 kDa, respectively (Zhou *et al.*, 1990; Iwahana *et al.*, 1993; Brayton *et al.*, 1994). The molecular masses for the chicken and rat enzymes include an 11-amino acid N-terminal propeptide while the size of the human enzyme is with this propeptide removed. Rowe and Wyngaarden (1968) reported the pigeon liver enzyme to have a molecular mass of 200 kDa, which could dissociate into species of 100 and 50 kDa, corresponding to a tetramer, dimer, and monomer, respectively. Holmes *et al.* (1973a) showed by sucrose density gradient centrifugation and gel filtration that partially purified human placental amido PRTase is found as a mixture of a 270 kDa form, which predominates when the enzyme is incubated with purine nucleotides, and a 133 kDa form, which exists in the presence of P-Rib-PP. Mammalian amido PRTase has not been purified to homogeneity due to extreme lability *in vitro* and the low levels of enzyme in cells. Levels of purine biosynthetic enzymes are much higher in avian liver because birds are uricotelic. Amido PRTase from *Bacillus subtilis* has an iron-sulfur center essential for catalytic function (Grandoni *et al.*, 1989); the human enzyme is also oxygen sensitive, suggesting that it too has an iron-sulfur center (Itakura & Holmes, 1979; Leff *et al.*, 1984).

P-Rib-PP is bound as a substrate for amido PRTase with positive cooperativity (Hill & Bennett, 1969; Wood & Seegmiller, 1973), and the purine nucleotides AMP, GMP, and IMP promote such cooperativity (Holmes *et al.*, 1973b; Tsuda *et al.*, 1979a,b). There is no evidence for cooperativity in the binding of L-glutamine. The binding of substrates to the enzyme is sequential with P-Rib-PP binding first (Hill & Bennett, 1969). The glutamine antagonists azaserine and 6-diazo-5-oxo-L-norleucine inactivate amido PRTase in the presence of P-Rib-PP but not in its absence (King *et al.*, 1978). Amido PRTase from mammalian sources is subject to feedback inhibition by AMP, IMP, and GMP (Itakura *et al.*, 1981), which accentuates the cooperativity with respect to P-Rib-PP and induces a transition from the active dimer to the inactive tetramer of the enzyme (Holmes, 1980).

† This investigation received financial support from National Health and Medical Research Council Project Grant 930019 and an Australian Research Council Institutional Grant.

⊗ Abstract published in *Advance ACS Abstracts,* May 1, 1997.

[1] Abbreviations: amido PRTase, 5-phosphoribosylamine:pyrophosphate phosphoribosyltransferase (EC 2.4.2.14); GAR, glycinamide riboside 5′-monophosphate; PRA, 5-phosphoribosylamine; P-Rib-PP, 5-phosphoribosyl 1-pyrophosphate.

S0006-2960(96)02598-6 CCC: $14.00

The anticancer drug, methotrexate, is a potent inhibitor of the enzyme dihydrofolate reductase (K_i = 4 pM; Thillet *et al.*, 1988), and the consequent accumulation of dihydrofolate polyglutamates (Allegra *et al.*, 1986) results in inhibition of the *de novo* purine pathway in mouse L1210 leukemia cells at reactions 1, 3 and 9 (Sant *et al.*, 1992).

P-Rib-PP → PRA → GAR → FGAR → FGAM → AIR → CAIR → SAICAR → AICAR → FAICAR → IMP (2)

Metabolic experiments with leukemia cells growing in culture showed that reaction 1, catalyzed by amido PRTase, is the primary site of inhibition of purine biosynthesis induced by methotrexate (Sant *et al.*, 1992). The pentaglutamyl derivative of dihydrofolate and the nonclassical antifolate piritrexim were found to be potent inhibitors of amido PRTase *in vitro*, while the pentaglutamyl derivative of methotrexate was far less effective (Sant *et al.*, 1992). In this paper, we investigate the mechanisms of inhibition of amido PRTase by piritrexim and AMP using enzyme kinetic techniques and sucrose density gradient centrifugation.

EXPERIMENTAL PROCEDURES

Materials and Methods. Mouse L1210 leukemia cells were provided by the Peter MacCallum Cancer Institute (Melbourne, Australia). *Escherichia coli* TX635/pJS187, which overproduces GAR synthetase, was obtained from Dr. J. Stubbe at the Massachusetts Institute of Technology (Boston, MA). RPMI 1640 medium and gentamycin were from the Sigma Chemical Co., (St. Louis, MO), and fetal calf serum was from the Commonwealth Serum Laboratories (Melbourne, Australia). L-[U-^{14}C]glutamine (0.447 mM, 224 Ci/mol) was from Du Pont (Sydney, Australia), and [1-^{14}C]-glycine (180 mM, 56 Ci/mol) and L-[*carboxy*-^{14}C]orotic acid (1.90 mM, 52.5 Ci/mol) were from Amersham International (Buckinghamshire, UK). Poly(ethylenimine)−cellulose thin-layer chromatograms were manufactured by Macherey-Nagel (Düren, Germany), and DEAE-Sephacel was from Pharmacia Fine Chemicals (Uppsala, Sweden). Dye reagent for protein assays was purchased from Bio-Rad Laboratories (Richmond, VA). Alcohol dehydrogenase, lactate dehydrogenase, and catalase for use as marker proteins in sucrose density gradient centrifugation were obtained from Sigma. Piritrexim was kindly donated by Burroughs Wellcome Co. (Research Triangle Park, NC) and by the National Cancer Institute (Bethesda, MD). All other chemicals were of the highest analytical grade commercially available.

Cell Culture. Mouse L1210 leukemia cells were grown in RPMI 1640 medium containing fetal calf serum (13% v/v), gentamicin (50 μg/mL), $NaHCO_3$ (500 μM), and K·Hepes, pH 7.45. Cells grew in angle-neck flasks or spinner flasks at 37 °C with a doubling time of 11 h. Cells were harvested in late exponential phase (9×10^5 cells/mL) by centrifugation (150*g*, 10 min, 4 °C) and washed twice with phosphate-buffered saline.

Partial Purification of Amido PRTase. All procedures were carried out at 0−4 °C. The cell pellet was resuspended in 2 volumes of 20 mM K·Hepes (pH 7.0), 0.25 M sucrose, 1.0 mM $MgCl_2$, and 1.0 mM DTT, and the cells were lyzed by sonication (30 W, 2 × 30 s). Cellular debris was removed by centrifugation (40000*g*, 45 min, 2 °C) and the cell-free extract was used immediately. Nucleic acids were removed by precipitation with 3.5% (w/v) streptomycin sulfate, which gave a minimal value for the absorbance ratio A_{260}/A_{280} of the cell extract after the precipitate was removed. Amido PRTase was further purified by fractionation with 40−60% (of saturation) ammonium sulfate. The desalted ammonium sulfate fraction was loaded onto a DEAE-Sephacel column (1.2 × 19 cm), and amido PRTase was eluted with a linear gradient of 0 to 300 mM KCl in 20 mM K·Hepes (pH 7.3), 1.0 mM $MgCl_2$, 10% (v/v) glycerol, and 1.0 mM DTT (90 mL). A major peak of amido PRTase eluted between 180 and 250 mM KCl which was pooled, concentrated, and desalted. The final enzyme preparation was purified 13-fold from the cell-free extract with a recovery of 41% of the enzymic activity. Analysis of each of the fractions in the purification procedure by SDS−PAGE is shown in Figure 1. The partially purified enzyme was stored at −80 °C prior to use.

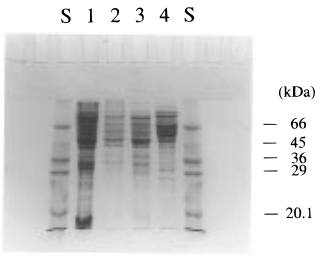

FIGURE 1: SDS−PAGE fractions from the partial purification of amido PRTase. Lane 1, crude mouse L1210 leukaemia cell extract; lane 2, streptomycin sulfate supernatant; lane 3, 40−60% ammonium sulfate fraction; lane 4, pooled fractions from DEAE-Sephacel containing amido PRTase activity; lane S, standard proteins are α-lactalbumin (M_r = 14 200), carbonic anhydrase (M_r = 29 000), glyceraldehyde-3-phosphate dehydrogenase (M_r = 36 000), ovalbumin (M_r = 45 000), and bovine albumin (M_r = 66 000). Proteins were separated using the discontinuous buffer system described by Laemmli (1970) with a 4% (w/v) acrylamide stacking gel and a 10% (w/v) acrylamide resolving gel. Proteins were stained with Coomassie blue R250.

Assay of Amido PRTase Activity. A modification of the procedure of Schendel *et al.* (1988) was used which couples the formation of PRA to production of GAR using an excess of pure recombinant GAR synthetase purified from *E. coli* (P-Rib-PP → PRA → GAR). Assay mixtures contained in a total volume of 25 μL: 50 mM K·Hepes (pH 7.2), 1.0 mM $MgCl_2$, P-Rib-PP, L-glutamine, 800 μM [^{14}C]glycine (20 Ci/mol), 500 μM MgATP, pure GAR synthetase (1.2 μg of protein), and amido PRTase. Saturating concentrations of P-Rib-PP and L-glutamine (500 μM and 3.0 mM, respectively) were used unless indicated otherwise. Assays were initiated by addition of amido PRTase, samples (7 μL) were taken at 5,10, and 15 min and applied to the origins of poly(ethyleneimine)-cellulose chromatograms (10 cm grooved into 1.5 cm channels). The sample spots were dried with cool air and immediately separated from [^{14}C]glycine by ascending chromatography with 0.34 M NaCl. The [^{14}C]-GAR was located by autoradiography ($R_f \approx 0.60$), excized, and quantified by scintillation counting. Initial reaction velocities were determined by linear regression of [^{14}C]GAR formed at 5, 10, and 15 min.

Analysis of Data. Kinetic data obtained for amido PRTase were fitted to appropriate velocity equations using the program DNRP53 for nonlinear regression analysis (Duggleby, 1984) with all data points given equal weighting. Kinetic models for amido PRTase assumed that the active

form of the enzyme is a dimer (Holmes, 1980), and the kinetic data were consistent with an ordered sequential mechanism with P-Rib-PP bound to the enzyme first (Hill & Bennett, 1969; Musick, 1981). For derivation of velocity equations, it was assumed that PRA was formed by one catalytic site with a first-order rate constant k, that all enzyme species are in rapid equilibrium, and that catalysis is the rate-limiting step (Segel, 1975). A complete derivation of the velocity equation describing the initial velocity pattern for substrates using the Rapid Equilibrium Assumption is available as Supporting Information.

In the presence of saturating concentrations of L-glutamine (B) the velocity equation as a function of P-Rib-PP concentration (A) is

$$\frac{\nu}{V_{max}} = \frac{\beta K_a A + A^2}{\beta K_a{}^2 + 2\beta K_a A + A^2} \quad (3)$$

where K_a is the dissociation constant for interaction of A with amido PRTase E and β is an interaction factor to account for the positive cooperativity for binding of a second molecule of A.

When the concentration of P-Rib-PP (A) is saturating, the velocity equation as a function of of L-glutamine concentration (B) is

$$\frac{\nu}{V_{max}} = \frac{\psi K_B B + B^2}{\psi K_B{}^2 + 2\psi K_B B + B^2} \quad (4)$$

where K_B is the dissociation constant for interaction of B with the EA complex and ψ is an interaction factor to account for any change in affinity for binding of a second molecule of L-glutamine (B) to dimeric amido PRTase.

For noncompetitive inhibition of amido PRTase by piritrexim (I), when the concentration of L-glutamine (B) is saturating and P-Rib-PP (A) is the varied substrate, the velocity equation is

$$\nu/V_{max} = \theta\epsilon^4 K_i{}^2(\beta K_a A + A^2)/[\theta\epsilon^4 K_i{}^2(\beta K_a{}^2 + 2\beta K_a A + A^2) + \theta\epsilon^2 K_i I(2\beta\epsilon^2 K_a{}^2 + 4\beta\epsilon K_a A + 2A^2) + I^2(\beta\epsilon^4 K_a{}^2 + 2\beta\epsilon^2 K_a A + A^2)] \quad (5)$$

where it is assumed that all enzyme−inhibitor complexes are catalytically inactive, β, ϵ, and θ are interaction factors as defined in Figure 2a, K_i is the dissociation constant for interaction of I with the free enzyme, and the other parameters of Figure 2a have been defined above.

For noncompetitive inhibition of amido PRTase by piritrexim (I) when P-Rib-PP (A) is saturating and L-glutamine (B) is varied

$$\nu/V_{max} = \theta\epsilon^4 K_I{}^2(\psi K_B B + B^2)/[\theta\epsilon^4 K_I{}^2(\psi K_B{}^2 + 2\psi K_B B + B^2) + \epsilon^2\theta K_I I(2\psi\epsilon^2 K_B{}^2 + 4\epsilon\psi K_B B + 2B^2) + I^2(\psi\epsilon^4 K_B{}^2 + 2\psi\epsilon^2 K_B B + B^2)] \quad (6)$$

where K_I is the dissociation constant for interaction of I with the enzyme−P-Rib-PP complex (AEA); the equilibria between enzyme forms are shown in Figure 2b.

For AMP (I) acting as a competitive inhibitor at low concentrations (0−125 μM) with respect to P-Rib-PP (A) of amido PRTase (E) in the presence of saturating L-glutamine (B), the velocity equation is

$$\nu/V_{max} = [\beta\sigma\omega K_a K_i{}^2 A + \sigma\omega K_i{}^2 A^2 + \beta\omega K_a K_i A I]/[\beta\sigma\omega K_a{}^2 K_i{}^2 + 2\beta\sigma\omega K_a K_i{}^2 A + \sigma\omega K_i{}^2 A^2 + 2\beta\sigma\omega K_a{}^2 K_i I + 2\beta\omega K_a K_i A I + \beta\sigma K_a{}^2 I^2] \quad (7)$$

where β, σ and ω are interaction factors defined in Scheme 1, K_a is the dissociation constant for interaction of A with E, and K_i, in this case, is the dissociation constant for interaction of I with the binding site for A. Although AMP induces formation of an inactive tetramer of amido PRTase (Holmes, 1980), it has been assumed for this analysis that the tetramer consists of two functional dimers.

For AMP (I) at higher concentrations (0−10 mM) acting as a noncompetitive inhibitor of amido PRTase with L-glutamine (B) as the varied substrate and saturating P-Rib-PP (A), the data were fitted to eq 6; the equilibria between enzyme forms are shown in Figure 2b.

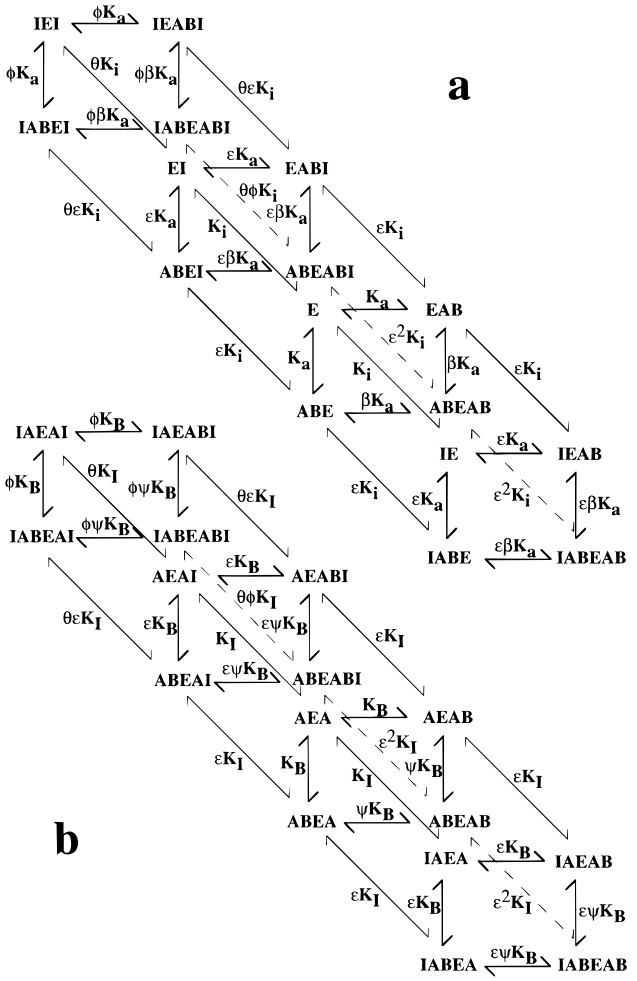

FIGURE 2: Kinetic models for allosteric inhibition of dimeric amido PRTase by piritrexim. All enzyme species are in rapid equilibrium, the enzyme−substrate complexes EAB, ABE, and ABEAB produce PRA with the first-order rate constant k or $2k$ for the latter fully saturated complex. All enzyme-inhibitor species are assumed to be completely catalytically inactive. Panel a is at saturating concentrations of L-glutamine (B, 3.0 mM) and K_a and K_i are dissociation constants. Panel b is at saturating concentrations of P-Rib-PP (A, 500 μM) and K_B and K_I are dissociation constants. The symbols β, ϵ, ϕ, ψ, and θ are interaction factors to allow for possible changes in affinity of different enzyme species for the same ligand.

Scheme 1

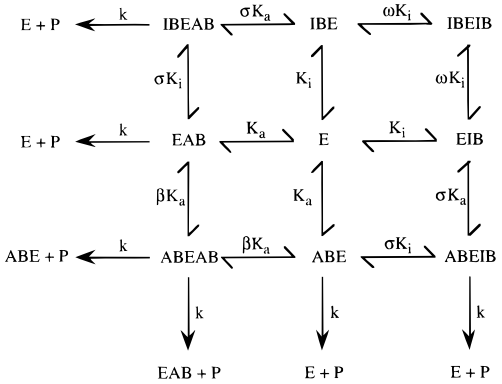

Sucrose Density Gradient Centrifugation. Linear sucrose gradients from 10 to 25% (w/v) were prepared using a SG15 gradient maker (Hoefer Scientific Instruments, San Francisco, CA). The sucrose gradients also contained in a volume of 11.6 mL, 20 mM K·Hepes (pH 7.3), 1.0 mM $MgCl_2$, 1.0 mM DTT, and other components (AMP, piritrexim, or P-Rib-PP) as required. Samples for centrifugation contained in a volume of 200 μL, partially purified murine amido PRTase (0.5 mg of protein), three marker proteins [alcohol dehydrogenase (1 mg), lactate dehydrogenase (150 μg), and catalase (500 μg)] with other components as indicated. These samples were incubated at 37 °C for 15 min prior to being layered onto the appropriate gradient of similar composition. Sedimentation profiles for amido PRTase were developed by centrifugation at 40000 rpm in a Beckman SW41 Ti rotor for 24 h at 4 °C using a Beckman L8-80M ultracentrifuge. Gradients were fractionated at 4 °C by puncturing the bottom of the tube; 320 μL fractions were collected and assayed immediately for amido PRTase. The sedimentation coefficient ($s_{20,w}$) of amido PRTase in the presence of effectors was determined from a calibration curve of the three standard proteins for each gradient using published $s_{20,w}$ values: horse liver alcohol dehydrogenase, 5.1 S; bovine heart lactate dehydrogenase, 7.0 S; and bovine liver catalase, 11.3 S (Smith, 1973). Marker proteins in gradient fractions were assayed by standard procedures: alcohol dehydrogenase by the increase in absorbance at 340 nm, lactate dehydrogenase by the decrease in absorbance at 340 nm, and catalase by the decrease in absorbance at 240 nm.

RESULTS

The coupled radioassay for amido PRTase utilizing thin layer chromatography on poly(ethyleneimine)-cellulose chromatograms enabled rapid analysis of the large number of assay samples generated in enzyme kinetic experiments. Progress curves for formation of [^{14}C]GAR were linear with respect to time, and plots of enzyme activity versus concentration of amido PRTase were also linear. For the kinetic studies reported here, experiments were performed in the presence of saturating concentrations of one of the substrates (500 μM P-Rib-PP or 3.0 mM L-glutamine) to reduce the number of possible enzyme species to be accounted for in velocity equations. Using this approach, it has been possible to obtain numerical values for all of the dissociation constants and interaction factors shown in Figure 2. Such values obtained for the substrates have been subsequently substituted into velocity equations describing inhibition by piritrexim and AMP, enabling dissociation constants and interaction factors to be obtained for these inhibitors by nonlinear regression.

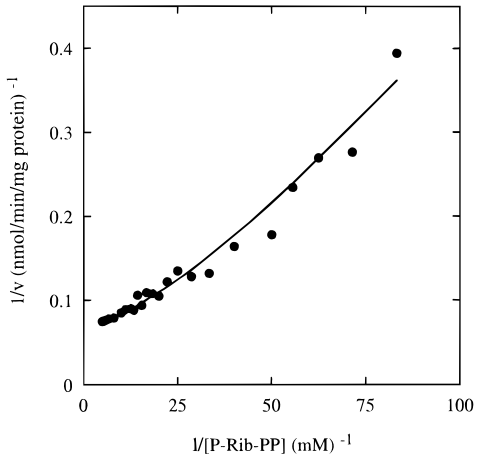

FIGURE 3: Lineweaver−Burk plot showing the dependence of amido PRTase activity on P-Rib-PP concentration. Assays contained 2.3 μg of protein, a saturating concentration of L-glutamine (3.0 mM), and P-Rib-PP at the indicated concentrations (1.0−450 μM) and were performed as described in Experimental Procedures. The data were fitted by nonlinear regression to eq 3, and the parameter values listed in the text were used to draw the line through the data.

Kinetic Analysis of the Substrates. The dependence of amido PRTase activity on the concentration of P-Rib-PP (1.0−450 μM) at a saturating concentration of L-glutamine (3.0 mM) is shown in Figure 3. The data were fitted to eq 3 which describes the panel of Figure 2a containing just enzyme−substrate complexes. The parameter values obtained (V_{max} = 14.7 ± 0.3 nmol/min/mg of protein, K_a = 80.4 ± 13.2 μM, and β = 0.192 ± 0.037) were used to draw the theoretical curve through the experimental data of Figure 3. The Lineweaver−Burk plot shows upward curvature consistent with the binding of P-Rib-PP with positive cooperativity. The dependence of amido PRTase activity on the concentration of L-glutamine (7.8−2340 μM) at a saturating concentration of P-Rib-PP (500 μM) was also determined.[2] Data were fitted to eq 4 which describes the panel of Figure 2b containing just enzyme−substrate complexes. The parameter values obtained (V_{max} = 16.6 ± 1.0 nmol/min/mg of protein, K_B = 327 ± 31 μM, and ψ = 1.18 ± 0.43) generated virtually a linear Lineweaver−Burk plot with minimal cooperativity for the binding of L-glutamine. Reaction velocities for amido PRTase at P-Rib-PP concentrations from 16.7 to 100 μM and L-glutamine concentrations from 300 to 600 μM were fitted to a velocity equation describing equilibria between all enzyme−substrate forms for a two-site model.[2] The parameter values obtained above were fixed in this equation using the nonlinear regression program, DNRP53, and a value for the interaction factor, α = 0.247 ± 0.042, was obtained describing the equilibrium EA ↔ AEA, with the dissociation constant αK_a indicating positive cooperativity. This value is comparable to that for β = 0.192 ± 0.037 for the equilibrium EAB ↔ ABEAB, with the dissociation constant βK_a.

Inhibition by Piritrexim. The spatial relationship of the inhibitory site for piritrexim to the catalytic site of the

[2] The equation describing the initial velocity pattern where the concentrations of P-Rib-PP and L-glutamine were varied, and the fitting of such data to this equation is available as Supporting Information.

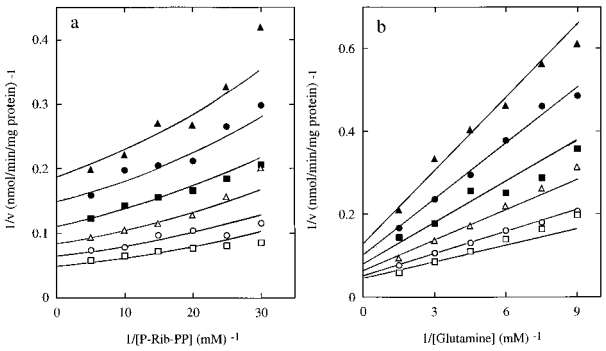

FIGURE 4: Inhibition of amido PRTase by piritrexim. Enzymic activity was determined at the indicated concentrations of (a) P-Rib-PP and (b) L-glutamine in the presence of the following concentrations of piritrexim: □, 0 μM; ○, 6 μM; △, 12 μM; ■, 18 μM; ●, 24 μM; ▲, 30 μM. The substrate not varied was at a saturating concentration: (a) 3.0 mM L-glutamine and (b) 500 μM P-Rib-PP. Assays contained 2.3 μg of protein, further details are described under Experimental Procedures. Data for panel a were fitted to eq 5 and data for panel b were fitted to eq 6, and the parameter values listed in the text were used to draw the lines.

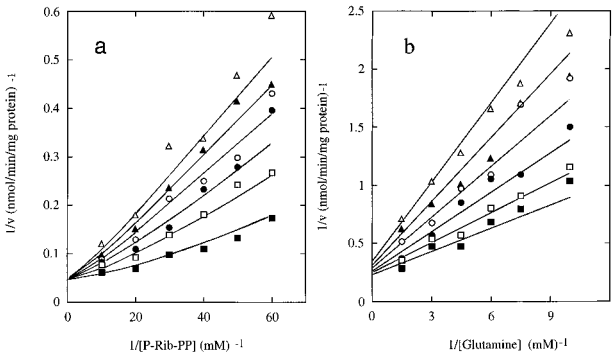

FIGURE 5: Inhibition of amido PRTase by AMP. Enzymic activity was determined at the indicated concentrations of (a) P-Rib-PP and (b) L-glutamine. (a) The following concentrations of AMP were used in the presence of saturating L-glutamine (3.0 mM) ■, 0 μM; □, 25 μM; ●, 50 μM; ○, 75 μM; ▲, 100 μM; △, 125 μM. (b) AMP concentrations in the presence of saturating P-Rib-PP (500 μM) were: ■, 0 mM; □, 2.0 mM; ●, 4.0 mM; ○, 6.0 mM; ▲, 8.0 mM; △, 10 mM. Assays contained 2.5 μg of protein, further details are described under Experimental Procedures. Data were fitted to eqs 7 and 6, respectively, the parameter values listed in the text were used to draw the lines.

enzyme was investigated with inhibition patterns for both substrates varied in turn at a saturating concentration of the other substrate (Figure 4). The data of Figure 4a, where L-glutamine is saturating, were fitted to eq 5, which is derived from the rapid equilibrium model of Figure 2a. Values for $K_a = 80.4$ μM and $\beta = 0.192$, determined above, were substituted into eq 5 to which the data of Figure 4a were fitted to yield the values $V_{max} = 20.4 \pm 0.4$ nmol/min/mg of protein, $K_i = 66.0 \pm 17.8$ μM, $\epsilon = 0.885 \pm 0.103$, and $\theta = 0.187 \pm 0.113$. Lines at higher piritrexim concentrations and lower P-Rib-PP concentrations show upward curvature, consistent with positive cooperativity with respect to P-Rib-PP. The data of Figure 4b where P-Rib-PP is saturating were fitted to eq 6, which is derived from the rapid equilibrium model of Figure 2b. Values for $K_B = 327$ μM and $\psi = 1.18$ determined above were substituted into eq 6 to which the data of Figure 4b were fitted to yield the values $V_{max} = 24.5 \pm 0.5$ nmol/min/mg of protein, $K_I = 62.3 \pm 15.6$ μM, $\epsilon = 1.17 \pm 0.10$, and $\theta = 0.0958 \pm 0.0585$. The parameter values obtained from the data of Figure 4 were used to draw the lines. Both inhibition patterns intersect to the left of the $1/v$ axis, indicating that piritrexim binds at a site distinct from the catalytic site.

Inhibition by AMP. The inhibition pattern of Figure 5a indicates that AMP is a competitive inhibitor with respect to P-Rib-PP of amido PRTase. With P-Rib-PP (16.7−100 μM) as the varied substrate, increasing concentrations of AMP (0−125 μM) and saturating L-glutamine (3.0 mM), the extrapolated lines from the experimental data intersected on the $1/v$ axis in three independent experiments. A rapid equilibrium model for all enzyme species is shown in Scheme 1 from which eq 7 was derived. Values for $K_a = 80.4$ μM and $\beta = 0.192$ obtained above were substituted into eq 7, and the data of Figure 5a were then fitted by nonlinear regression to yield values of $V_{max} = 21.4 \pm 0.5$ nmol/min/mg of protein, $K_i = 40.0 \pm 8.1$ μM, $\sigma = 0.641 \pm 0.157$, and $\omega = 1.78 \pm 1.18$. These values were used to draw the theoretical lines through the data. The data did not fit to an equation describing noncompetitive binding of AMP at saturating L-glutamine concentrations. Inhibition patterns for amido PRTase with L-glutamine (100−667 μM) as the varied substrate, increasing concentrations of AMP (0−10 mM), and saturating P-Rib-PP (500 μM) indicated noncompetitive inhibition (Figure 5b). AMP could not bind at the catalytic site for P-Rib-PP in the presence of saturating concentrations of this substrate, and much higher concentrations of AMP (0−10 mM) were required for the noncompetitive inhibition, suggesting that AMP is binding at a second low-affinity site which is distinct from the catalytic site. This type of inhibition (Figure 5b) is consistent with the model of Figure 2b already used for noncompetitive inhibition of the enzyme by piritrexim with L-glutamine as the varied substrate (Figure 4b). The data of Figure 5b were therefore fitted to eq 6 with the fixed values, $K_B = 327$ μM and $\Psi = 1.18$ determined above, to yield the values $V_{max} = 4.96 \pm 0.12$ nmol/min/mg of protein, $K_I = 16.4 \pm 5.2$ mM, $\epsilon = 1.61 \pm 0.26$, and $\theta = 0.286 \pm 0.275$. These parameter values were used to draw the lines of Figure 5b.

Effects of Ligands on the Sedimentation Coefficient of Amido PRTase. In agreement with Holmes *et al.* (1973a), sedimentation of amido PRTase through sucrose gradients in the presence of AMP and P-Rib-PP induced two distinct states of aggregation (Figure 6). In the presence of 5 mM AMP, the tetrameric form of amido PRTase was induced with a sedimentation coefficient of 10.2 ± 0.4 S ($n = 3$, Figure 6a): GMP had a similar effect (data not shown). The presence of 250 μM P-Rib-PP promoted the formation of a dimeric form of the enzyme with a sedimentation coefficient of 6.7 ± 0.3 S ($n = 3$, Figure 6d). In the absence of effectors, the peak for amido PRTase was broader and less symmetrical, giving an apparent $s_{20,w}$ value of 9.3 ± 0.6 S ($n = 3$, Figure 6b). The weighting of this peak indicates a predominance of the tetrameric form. The two aggregation states of the enzyme are interconvertible and would be in dynamic equilibrium during centrifugation, resulting in the observed broad profile. When amido PRTase was incubated with 100 μM piritrexim, the enzyme sedimented with a limiting $s_{20,w}$ value of 7.2 ± 0.5 S ($n = 3$, Figure 6c). Amido PRTase was preincubated with 0, 2, 5, 10, 20, and 100 μM piritrexim and then sedimented through six gradients of similar composition. The apparent sedimentation coefficient decreased progressively from 9.3 S, as isolated from mouse leukaemia cells, to the limiting value of 7.2 S with 100 μM

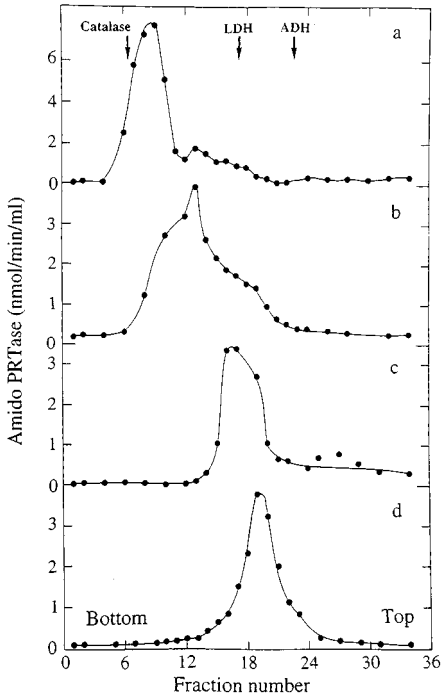

FIGURE 6: Sucrose density gradient centrifugation of amido PRTase in the presence of AMP, piritrexim, or P-Rib-PP. Partially purified amido P′RTase (0.5 mg of protein) was preincubated at 37 °C for 30 min with the appropriate effector and then sedimented through a density gradient of 10 to 25% (w/v) sucrose containing 20 mM K·Hepes (pH 7.3), 1.0 mM $MgCl_2$, 1.0 mM DTT, and (a) 5.0 mM AMP, (b) control, (c) 100 μM piritrexim, and (d) 250 μM P-Rib-PP. The positions of the protein standards catalase, lactate dehydrogenase (LDH), and alcohol dehydrogenase (ADH) are indicated as is the top and bottom of the centrifuge tube. Further details of centrifugation, fractionation and enzyme assays appear in Experimental Procedures.

piritrexim. Piritrexim is a potent inhibitor of amido PRTase (K_i = 6.0 μM; Sant *et al.*, 1992), and the results indicate formation of an inactive 7.2 S dimer with a different conformation to the active 6.7 S species. Amido PRTase preincubated with a mixture of 2.5 mM AMP and 50 μM piritrexim, sedimented through a gradient containing both effectors with a velocity between that of the large and small forms of the enzyme (Figure 7).

DISCUSSION

The use of a sensitive radioassay has enabled a detailed kinetic analysis of the interaction of inhibitors with amido PRTase. Dissociation constants for the substrates P-Rib-PP and L-glutamine have been determined as K_a = 80.4 μM (E + A ↔ EA) and K_b = 421 μM (EA + B ↔ EAB). Both values are lower than those previously reported for mammalian amido PRTase (Holmes, 1980). Positive cooperativity was found for P-Rib-PP with α = 0.247 (EA + A ↔ AEA). Thus, the dissociation constant for binding the second molecule of P-Rib-PP to amido PRTase is αK_a = 19.8 μM. Values obtained for the dissociation constants of substrates were then used in subsequent analyses to determine the dissociation constants and interaction factors for the inhibitors, piritrexim, and AMP. Inhibition patterns for piritrexim indicate that this nonclassical antifolate acts as a noncompetitive inhibitor of amido PRTase, consistent with a distinct inhibitory allosteric site for folate derivatives. Dissociation constants for piritrexim, determined from the two inhibition patterns with each substrate varied, are similar (E + I ↔ EI, 66.0 μM; AEA + I ↔ AEAI, 62.3 μM, Figure 4a,b); the values of 0.187 and 0.0958 obtained for the interaction factor θ indicate strong positive cooperativity for the binding of piritrexim. The dissociation constants for the second interaction of piritrexim with amido PRTase would be θK_i = 12.3 μM and θK_I = 5.97 μM respectively, for the two sets of data, consistent with an apparent inhibition constant for piritrexim reported by Sant *et al.* (1992) of 6.0 μM. Dixon plots ($1/v$ versus [piritrexim]) showed upward curvature (Sant *et al.*, 1992), again consistent with positive cooperativity for the binding of piritrexim.

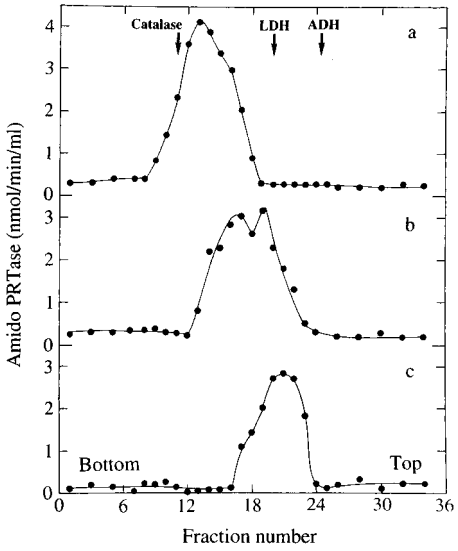

FIGURE 7: Interconversion between the large and small forms of amido PRTase induced by AMP and piritrexim. Amido PRTase (0.5 mg of protein) was sedimented through sucrose gradients containing the appropriate effector as for Figure 5: (a) 5.0 mM AMP, (b) 2.5 mM AMP and 50 μM piritrexim, and (c) 100 μM piritrexim.

The inhibition pattern for AMP with P-Rib-PP as the varied substrate is consistent with AMP binding as a competitive inhibitor with K_i = 40.0 μM (E + I ↔ EI, Figure 5a). This conclusion is consistent with previous reports that inhibition by purine nucleotides is competitive with respect to P-Rib-PP (Wood & Seegmiller, 1973; Messenger & Zalkin, 1979), although a detailed kinetic analysis was not reported. Experiments by Tsuda *et al.* (1979b) showed that the inhibition by purine nucleotides could be completely overcome by adding a high concentration of P-Rib-PP. Data presented here suggest that AMP at low concentrations (0−125 μM) acts as an analog of P-Rib-PP, thus competing for the substrate binding site. Smith *et al.* (1994) determined the three-dimensional structure of amido PRTase from *Bacillus subtilis* by multiwavelength anomalous diffraction and proposed that this metalloenzyme is a paradigm for the higher eukaryotic enzymes which have not been purified in active form. The *B. subtilis* enzyme crystallized as a tetramer and bound eight molecules of AMP in two types of binding sites. AMP bound at the P-Rib-PP catalytic site, as concluded from the data of Figure 5a, and at an unusual regulatory site between the subunits. The AMP bound at this second site of the bacterial enzyme also appeared to overlap part of the catalytic site for P-Rib-PP. For the mouse enzyme, AMP at higher concentrations (0−10 mM) acts as a noncompetitive inhibitor with respect to L-glutamine with a dissociation constant of 16.4 mM (AEA + I ↔ AEAI, Figure 5b). The dissociation constants obtained for AMP

with P-Rib-PP or L-glutamine as the varied substrate (Figure 5a,b) of 40.0 μM or 16.4 mM, respectively, indicate that AMP binds at two distinct sites, perhaps with a similar arrangement to the bacterial enzyme (Smith *et al.*, 1994). The inhibition of amido PRTase by AMP (IMP and GMP) would be further complicated by formation of the inactive tetramer at higher concentrations of AMP (Figures 6 and 7).

Sucrose density gradient experiments with amido PRTase from mouse L1210 leukemia cells have shown the existence of three forms of the enzyme. The substrate P-Rib-PP induces formation of a small, active form (6.7 S); the folate analog piritrexim induces a small, inactive form (7.2 S); and AMP induces a large inactive form (10.2 S). It is assumed that the small forms are dimers and the large form is a tetramer. The small active form and the large inactive form were identified by Holmes *et al.* (1973a), but the small inactive form (7.2 S) induced by piritrexim has not been reported. Instability of the mammalian enzyme has precluded its isolation in pure form. The 7.2 S form of amido PRTase found in the presence of piritrexim could therefore consist of one amido PRTase subunit and a second different subunit which binds piritrexim. Smith *et al.* (1994) found no evidence for an inhibitory allosteric site for folate derivatives on the amido PRTase from *B. subtilis*, although the relationship between this bacterial enzyme and the mammalian enzyme may not be sufficiently close. Amido PRTase from mouse L1210 leukemia cells is subject to potent inhibition by the pentaglutamyl derivative of dihydrofolate (apparent $K_i = 3.1$ μM) and piritrexim (apparent $K_i = 6.0$ μM; Sant *et al.*, 1992). Dihydrofolate is too unstable to use in sucrose density gradients but it is assumed that both folate derivatives would have similar effects on the enzyme. The identity of the subunit which contains the inhibitory allosteric site for piritrexim (and dihydrofolate polyglutamates) must await the isolation of mammalian amido PRTase in pure and active form.

ACKNOWLEDGMENT

We thank Dr. J. Stubbe of the Massachusetts Institute of Technology for *E. coli* TX635/pJS187 which overproduces GAR synthetase and Anne Madden for preparing the manuscript.

SUPPORTING INFORMATION AVAILABLE

Equations are derived describing the initial velocity pattern where the concentrations of P-Rib-PP and L-glutamine were varied, from which the equations for the limiting cases of saturating concentrations of L-glutamine (eq 3) and saturating P-Rib-PP (eq 4) are derived. Data for an initial velocity pattern for substrates are fitted to the appropriate equation to determine some of the kinetic parameters used in this paper. Similar procedures using the Rapid Equilibrium Assumption (Segel, 1975) were used to derive eqs 5, 6, and 7 (8 pages). Ordering information is given on any current masthead page.

REFERENCES

Allegra, C. J., Fine, R. L., Drake, J. C., & Chabner, B. A. (1986) *J. Biol. Chem. 261*, 6478−6485.
Brayton, K. A., Chen, Z., Zhou, G., Nagy, P. L., Gavalas, A., Trent, J. M., Deaven, L. L., Dixon, J. E., & Zalkin, H. (1994) *J. Biol. Chem. 269*, 5313−5321.
Duggleby, R. G. (1984) *Comput. Biomed. Res. 14*, 447−455.
Grandoni, J. A., Switzer, R. L., Makaroff, C. A., & Zalkin, H. (1989) *J. Biol. Chem. 264*, 6058−6064.
Hartman, S. C. (1963) *J. Biol. Chem. 238*, 3024−3035.
Hill, D. L., & Bennett, L. L., Jr. (1969) *Biochemistry 8*, 122−130.
Holmes, E. W. (1980) *Adv. Enzyme Reg. 19*, 215−231.
Holmes, E. W., Wyngaarden, J. B., & Kelley, W. N. (1973a) *J. Biol. Chem. 248*, 6035−6040.
Holmes, E. W., McDonald, J. A., McCord, J. M., Wyngaarden, J. B., & Kelley, W. N. (1973b) *J. Biol. Chem. 248*, 144−150.
Itakura, M., & Holmes, E. W. (1979) *J. Biol. Chem. 254*, 333−338.
Itakura, M., Sabina, R. L., Heald, P. W., & Holmes, E. W. (1981) *J. Clin. Invest. 67*, 994−1002.
Iwahana, H., Yamaoka, T., Mizutani, M., Mizusawa, N., Ii, S., Yoshimoto, K., & Itakura, M. (1993) *J. Biol. Chem. 268*, 7225−7237.
King, G. L., Bouhous, C. G., & Holmes, E. W. (1978) *J. Biol. Chem. 253*, 3933−3938.
Laemmli, V. K. (1970) *Nature 227*, 680−685.
Leff, R. L., Itakura, M., Udom, A., & Holmes, E. W. (1984) *Adv. Enzyme Reg. 22*, 403−411.
Messenger, L. J., & Zalkin, H. (1979) *J. Biol. Chem. 254*, 3382−3392.
Musick, D. L. (1981) *CRC Crit. Rev. Biochem. 11*, 1−34.
Rowe, P. B., & Wyngaarden, J. B. (1968) *J. Biol. Chem. 243*, 6373−6383.
Sant, M. E., Lyons, S. D., Phillips, L., & Christopherson, R. I. (1992) *J. Biol. Chem. 267*, 11038−11045.
Schendel, F. J., Cheng, Y. S., Otvos, J. D., Wehrli, S., & Stubbe, J. (1988) *Biochemistry 27*, 2614−2623.
Segel, I. H. (1975) *Enzyme Kinetics*, pp 560−593, John Wiley & Sons, New York.
Smith, M. H. (1973) in *Handbook of Biochemistry* (Sober, H. A., Ed.) pp C11−C19, Chemical Rubber Publishing Co., Cleveland, OH.
Smith, J. L., Zaluzec, E. J., Wery, J.-P., Niu, L., Switzer, R. L., Zalkin, H., & Satow, Y. (1994) *Science 264*, 1427−1433.
Thillet, J., Absil, J., Stone, S. R., & Pictet, R. (1988) *J. Biol. Chem. 263*, 12500−12508.
Tsuda, M., Katunuma, N., Morris, H. P., & Weber, G. (1979a) *Cancer Res. 39*, 305−311.
Tsuda, M., Katunuma, N., & Weber, G. (1979b) *J. Biochem. 85*, 1347−1354.
Wood, A. W., & Seegmiller, J. E. (1973) *J. Biol. Chem. 248*, 138−143.
Zhou, G. Dixon, J. E., & Zalkin, H. (1990) *J. Biol. Chem. 265*, 21152−21159.

BI962598M